

# A ROBUST AND HIGH PRECISION ALGORITHM FOR ELASTIC SCATTERING PROBLEMS FROM CORNERED DOMAINS

JIANAN YAO, BAOLING XIE, AND JUN LAI

**ABSTRACT.** The Navier equation is the governing equation of elastic waves, and computing its solution accurately and rapidly has a wide range of applications in geophysical exploration, materials science, etc. In this paper, we focus on the efficient and high-precision numerical algorithm for the time harmonic elastic wave scattering problems from cornered domains via the boundary integral equations in two dimensions. The approach is based on the combination of Nyström discretization, analytical singular integrals and kernel-splitting method, which results in a high-order solver for smooth boundaries. It is then combined with the recursively compressed inverse preconditioning (RCIP) method to solve elastic scattering problems from cornered domains. Numerical experiments demonstrate that the proposed approach achieves high accuracy, with stabilized errors close to machine precision in various geometric configurations. The algorithm is further applied to investigate the asymptotic behavior of density functions associated with boundary integral operators near corners, and the numerical results are highly consistent with the theoretical formulas.

## 1. INTRODUCTION

The analysis and computation of elastic scattering have received ever-increasing attention due to the applications in many important areas such as geological exploration, nondestructive testing, and materials science [1, 5, 21, 22, 24]. An accurate and efficient numerical method plays a pivotal role in many of these applications. For instance, in the inverse elastic obstacle scattering, often a large number of forward solving is required for methods based on the gradient descent [10]. This paper is concerned with the scattering of a time-harmonic incident wave in a cornered domain filled with a homogeneous and isotropic elastic medium in two dimensions. In particular, we develop a robust and highly accurate numerical method for solving the elastic scattering problems from cornered domains under Dirichlet and Neumann boundary conditions.

Cornered domains, characterized by sharp corners or edges in their boundaries, present unique challenges and opportunities for understanding the behavior of elliptic and wave equations [4, 13]. It is well-known that the interplay between the geometry of the domain and the inherent properties of wave equations gives rise to fascinating scattering phenomena, such as corner singularities and diffraction effects [12]. These singularities significantly impact the solutions of the governing equations and increase the difficulties of designing effective numerical schemes. Hence, although there are many computational methods available for the scattering problems of elastic waves [3, 8, 25, 26], most of them focus on smooth domains. Among them, the method of boundary integral equations (BIE) [9] offers an attractive approach for solving the elastic boundary value problems. The advantages of BIE are that the discretization is only needed on the boundary of the domain when the medium is homogeneous, reducing the dimension of computational domain by one, and the radiation condition at infinity is satisfied exactly for exterior scattering problems. However, solving the BIE

---

*Date:* October 18, 2023.

*2020 Mathematics Subject Classification.* 35J05, 45L05, 45E05, 65R20, 75B05.

*Key words and phrases.* elastic wave scattering, boundary integral equations, Nyström method, Navier equations, kernel-splitting method, RCIP method.

The work of JL was partially supported by the Key Project of Joint Funds for Regional Innovation and Development (No. U21A20425), NSFC grant No. 12371427 and the “Xiaomi Young Scholars” program from Xiaomi Foundation.

to high precision in cornered domains is highly nontrivial due to the singular integrals and corner singularities. One usually needs to put a very dense mesh near the corner in order to fully resolve the singularities, which leads to a large, dense and ill-conditioned linear system. Direct inversion suffers from severe numerical loss. Over the years, several approaches have been proposed to overcome this difficulty, including the  $L^2$  weighting method [6], corner rounding method [12], analytic expansion method [30], and recursively compressed inverse preconditioning (RCIP) [15], etc. Among them, of particular interest is the method of RCIP, initially proposed in [16], which has demonstrated high stability and accuracy for solving the second kind boundary integral equations in cornered domains. However, these methods predominantly focus on the Laplace and Helmholtz equations. Extension to elastic scattering is still challenging due to the complicated interconnection between compressional and shear waves [23]. In particular, since the elastic Green's function is given by a second-order tensor, the decomposition of singular kernels in the elastic BIE is highly nontrivial [11]. Existing decomposition methods are often ineffective for high-order discretization, especially in cornered domains.

In this paper, we propose an effective solver for the elastic scattering problems from cornered domains. The method is based on the combination of Nyström discretization, analytical singular integrals and kernel splitting method, which leads to a high-order solver for smooth geometries. When the boundary is piecewise smooth, we apply the non-uniform discretization with RCIP to fully resolve the corner singularities. Particularly, we give a novel decomposition of the singular kernels for elastic integral boundary operators, which is highly compact and easy to compute, and develop a high-order numerical discretization scheme for the singular integrals. In the end, we demonstrate the effectiveness of the proposed approach through various numerical examples, and verify the leading order singularities for the density functions of BIE near corners.

This paper is organized as follows. In Section 2, we formulate the time harmonic elastic scattering problems in two dimensions and show the singular behavior of the solution for the elastic scattering near the corner. In Section 3, we introduce the elastic potential theory and derive the decompositions of kernel functions in elastic boundary integral operators based on the asymptotic analysis. In Section 4, a high-order numerical discretization method for the elastic BIE in cornered domains is proposed, which combines the Nyström discretization, singular integral quadrature and the recursively compressed inverse preconditioning. In Section 5, several numerical examples are given to illustrate the effectiveness of the proposed method. The paper is concluded in Section 6.

## 2. PROBLEM FORMULATION

Consider a region  $\Omega \subset \mathbb{R}^2$  with a piecewise smooth boundary  $\Gamma$ . We assume the number of corner points on  $\Gamma$  is finite and  $\Omega$  is locally diffeomorphic in the neighborhood of every corner point to an infinite cone with an opening angle  $\theta_c \notin \{0, 2\pi\}$ . Denote  $\mathbf{n} = (n_1, n_2)^\top$  and  $\boldsymbol{\tau} = (\tau_1, \tau_2)^\top$  the unit normal and tangential vectors on  $\Gamma$ , respectively, where  $\tau_1 = -n_2, \tau_2 = n_1$ . Assume  $\Omega$  is filled with a homogeneous and isotropic elastic medium and illuminated by an elastic incident wave  $\mathbf{u}^{inc}$ . The total field  $\mathbf{u} = (u_1, u_2)^\top$  satisfies the time-harmonic (with time dependence  $e^{-i\omega t}$ ) Navier equation

$$\mu \Delta \mathbf{u} + (\lambda + \mu) \nabla (\nabla \cdot \mathbf{u}) + \rho \omega^2 \mathbf{u} = 0, \quad \mathbf{x} \in \Omega, \quad (1)$$

where  $\mu$  and  $\lambda$  are Lamé coefficients (with  $\mu > 0$  and  $\lambda + \mu > 0$ ),  $\rho$  is the mass density, and  $\omega$  is the angular frequency. Throughout, we assume all the material parameters are constant.

The total field  $\mathbf{u}$  in equation (1) is consisted of the incident field  $\mathbf{u}^{inc}$  and the scattered field  $\mathbf{u}^{sc}$ . There are typically two types of incident wave. One is the plane wave, which is a linear combination of the time-harmonic compressional plane wave  $\mathbf{d} e^{ik_p \mathbf{d} \cdot \mathbf{x}}$  and the shear plane wave  $\mathbf{d}^\perp e^{ik_s \mathbf{d} \cdot \mathbf{x}}$ , where  $\mathbf{d} = (\cos \theta, \sin \theta)^\top$  is the unit propagation direction vector,  $\theta \in [0, 2\pi)$  is the

incident angle,  $\mathbf{d}^\perp = (-\sin \theta, \cos \theta)^\top$  is an orthonormal vector of  $\mathbf{d}$ , and

$$k_p = \omega \sqrt{\frac{\rho}{\lambda + 2\mu}}, \quad k_s = \omega \sqrt{\frac{\rho}{\mu}},$$

are the compressional and shear wavenumber, respectively. Another type of incident wave is the point source, which is given by equation (9) in the next section. Both of them satisfy the Navier equation (1) globally except at the source point.

Our main concern is to find the scattered field  $\mathbf{u}^{sc}$  effectively from the cornered domains. The property of  $\mathbf{u}^{sc}$  depends on the boundedness of domain  $\Omega$ . Here we refer the elastic scattering problem as the interior problem if  $\Omega$  is bounded, and call it the exterior problem if  $\mathbb{R}^2 \setminus \overline{\Omega}$  is bounded.

**2.1. Interior elastic scattering problems.** We are concerned with two types of elastic scattering problems depending on the boundary condition of  $\Gamma$ .

*Interior Dirichlet problems:* When the exterior of  $\Omega$  is rigid, no deformation displacement occurs on the boundary  $\Gamma$ . Therefore, the total field  $\mathbf{u}$  satisfies

$$\mathbf{u} = 0, \quad \mathbf{x} \in \Gamma,$$

through which the scattered field  $\mathbf{u}^{sc}$  satisfies the Dirichlet boundary value problem

$$\begin{cases} \mu \Delta \mathbf{u}^{sc} + (\lambda + \mu) \nabla (\nabla \cdot \mathbf{u}^{sc}) + \rho \omega^2 \mathbf{u}^{sc} = 0, & \text{in } \Omega, \\ \mathbf{u}^{sc} = -\mathbf{u}^{inc}, & \text{on } \Gamma. \end{cases} \quad (2)$$

*Interior Neumann problems:* Given a vector function  $\mathbf{v} = (v_1, v_2)^\top$  and a scalar function  $v$ , we define the scalar and vector curl operators by

$$\text{curl} \mathbf{v} = \partial_{x_1} v_2 - \partial_{x_2} v_1, \quad \mathbf{curl} v = (\partial_{x_2} v, -\partial_{x_1} v)^\top,$$

respectively. The traction operator  $\mathcal{T}$  on  $\Gamma$  is defined by

$$\mathcal{T} \mathbf{u} = 2\mu \frac{\partial \mathbf{u}}{\partial \mathbf{n}} + \lambda (\nabla \cdot \mathbf{u}) \mathbf{n} - \mu \tau \text{curl} \mathbf{u}. \quad (3)$$

We call that  $\Gamma$  is traction free if

$$\mathcal{T} \mathbf{u} = 0, \quad \mathbf{x} \in \Gamma.$$

In this case, the scattered field  $\mathbf{u}^{sc}$  satisfies the Neumann boundary value problem

$$\begin{cases} \mu \Delta \mathbf{u}^{sc} + (\lambda + \mu) \nabla (\nabla \cdot \mathbf{u}^{sc}) + \rho \omega^2 \mathbf{u}^{sc} = 0, & \text{in } \Omega, \\ \mathcal{T} \mathbf{u}^{sc} = -\mathcal{T} \mathbf{u}^{inc}, & \text{on } \Gamma. \end{cases} \quad (4)$$

**2.2. Exterior boundary value problems.** For the elastic scattering in an unbounded domain, one can first decompose the scattered field  $\mathbf{u}^{sc}$  as

$$\mathbf{u}^{sc} = \mathbf{u}_p + \mathbf{u}_s, \quad (5)$$

with

$$\mathbf{u}_p = -\frac{1}{k_p^2} \nabla (\nabla \cdot \mathbf{u}^{sc}), \quad \mathbf{u}_s = \frac{1}{k_s^2} \mathbf{curl} \text{curl} \mathbf{u}^{sc}, \quad (6)$$

where  $\mathbf{u}_p$  is called the compressional wave, and  $\mathbf{u}_s$  is the shear wave. Equation (6) is the Helmholtz decomposition of the scattered field  $\mathbf{u}^{sc}$  [23], as in the two dimensions both  $\mathbf{u}_p$  and  $\mathbf{u}_s$  satisfy the Helmholtz equation with wavenumber  $k_p$  and  $k_s$  respectively. The *Exterior Dirichlet problems* and *Exterior Neumann problems* are given the same as (2) and (4), but coupled with the Kupradze-Sommerfeld radiation condition at infinity

$$\lim_{r \rightarrow \infty} r^{1/2} \left( \frac{\partial \mathbf{u}_p}{\partial r} - ik_p \mathbf{u}_p \right) = 0, \quad \lim_{r \rightarrow \infty} r^{1/2} \left( \frac{\partial \mathbf{u}_s}{\partial r} - ik_s \mathbf{u}_s \right) = 0, \quad r = |\mathbf{x}|. \quad (7)$$

**2.3. Corner singularity.** When the boundary  $\Gamma$  is smooth, the existence and uniqueness for the solutions of the elastic boundary value problems have been well established in [21]. In particular, for the interior boundary value problems, when the wavenumber  $k_p > 0$  and  $k_s > 0$ , there exists a unique solution in the space of  $(C^2(\Omega) \cap C^1(\overline{\Omega}))^2$  to equations (2) and (4) except a countable set of  $k_p$  and  $k_s$ . These special wavenumbers are called the interior Dirichlet and Neumann eigenvalues, respectively. For the exterior problems, as long as the wavenumbers  $k_p$  and  $k_s$  are positive, there always exists a unique solution that satisfies the equations (2) and (4) coupled with the radiation condition (7). Throughout this paper, unless otherwise stated, we only consider the regular wavenumbers by explicitly excluding these eigenvalues, so that the interior and exterior problems always admit a unique solution.

In case the boundary is piecewise smooth, due to the corner singularity, the solution for (2) and (4) only uniquely exists in some weighted Sobolev spaces [5]. In particular, the behavior of the solution  $\mathbf{u}^{sc}$  for the boundary value problems (2) or (4) in a neighborhood of the corner point can be described with the help of solutions of a homogeneous boundary value problem for the Lamé operator [17] in the infinite sector with the opening angle  $\theta_c$ . It was shown in [29] that the set of all solutions of this homogeneous problem has a basis consisting of the so-called ‘‘power solutions’’

$$u(r, \theta) \sim \sum_{j=1}^N \sum_{k=1}^{m_j} \sum_{l=0}^{\kappa_{j,k}} a_{j,k,l} r^{\alpha_j} \sum_{s=0}^l (\log r)^s \omega_j^{l-s,k}(\theta) + O(r), \quad (8)$$

where  $(r, \theta)$  with  $0 \leq \theta \leq \theta_c$  are polar coordinates with origin at the corner point and  $\{\omega_j^{l,k}, 1 \leq k \leq m_j, 0 \leq l \leq \kappa_{j,k}\}$  is a canonical system of Jordan chains of some linear operator pencil  $A$  [27] corresponding to the eigenvalue  $\alpha_j$ . Here  $m_j$  is the geometric multiplicity of  $\alpha_j$  and  $\kappa_{j,k} + 1$  is the length of the  $k$ th Jordan chain. The number  $N$  is chosen such that  $0 < \text{Re}(\alpha_j) < 1$ .

Due to the singularity at the corner, standard numerical method based on uniform mesh is usually inefficient and low order. Mesh refinement near the corner is unavoidable in numerical computations (except methods based on the analytical expansion [30]), which on the other hand causes numerical instability and generates a large linear system. To address these issues, we propose a robust and high-order numerical method to solve both the Dirichlet problems (2) and Neumann problems (4) in cornered domains based on the boundary integral equations.

### 3. POTENTIAL THEORY AND ASYMPTOTIC ANALYSIS

The boundary integral equation for elastic scattering is based on the potential theory of Navier equations. Given  $\mathbf{x} := (x_1, x_2)^\top$  and  $\mathbf{y} := (y_1, y_2)^\top$  with  $\mathbf{x} \neq \mathbf{y}$ , the free space Green’s function for equation (1) in two dimensions is given by

$$\mathbf{G}(\mathbf{x}, \mathbf{y}) = \frac{i}{4\mu} \left\{ H_0^{(1)}(k_s |\mathbf{x} - \mathbf{y}|) \mathbf{I} + \frac{1}{k_s^2} \nabla_{\mathbf{x}} \nabla_{\mathbf{x}}^\top \left( H_0^{(1)}(k_s |\mathbf{x} - \mathbf{y}|) - H_0^{(1)}(k_p |\mathbf{x} - \mathbf{y}|) \right) \right\}, \quad (9)$$

where  $H_0^{(1)}$  is the first kind Hankel function of order zero, and  $\mathbf{I}$  is the  $2 \times 2$  identity matrix.

When  $\omega = 0$ , equation (1) becomes the Lamé system [17] and the corresponding Green’s function is

$$\mathbf{E}(\mathbf{x}, \mathbf{y}) = \frac{\lambda + 3\mu}{4\pi\mu(\lambda + 2\mu)} \left\{ \gamma(\mathbf{x}, \mathbf{y}) \mathbf{I} + \frac{\lambda + \mu}{\lambda + 3\mu} \frac{1}{r^2} (\mathbf{x} - \mathbf{y})(\mathbf{x} - \mathbf{y})^\top \right\}, \quad (10)$$

with

$$\gamma(\mathbf{x}, \mathbf{y}) = -\ln |\mathbf{x} - \mathbf{y}|.$$

Let  $\boldsymbol{\varphi} = [\varphi_1, \varphi_2]^\top$  be a vector function defined on  $\Gamma$ . The single layer potential operator  $S$  is defined by

$$S[\boldsymbol{\varphi}](\boldsymbol{x}) = \int_{\Gamma} \mathbf{G}(\boldsymbol{x}, \boldsymbol{y}) \boldsymbol{\varphi}(\boldsymbol{y}) ds_{\boldsymbol{y}}, \quad \boldsymbol{x} \notin \Gamma. \quad (11)$$

When  $\boldsymbol{x}$  approaches the boundary  $\Gamma$ , it becomes the single layer boundary operator

$$\mathcal{S}[\boldsymbol{\varphi}](\boldsymbol{x}) = \int_{\Gamma} \mathbf{G}(\boldsymbol{x}, \boldsymbol{y}) \boldsymbol{\varphi}(\boldsymbol{y}) ds_{\boldsymbol{y}}, \quad \boldsymbol{x} \in \Gamma. \quad (12)$$

The double layer potential operator  $D$  is defined by

$$D[\boldsymbol{\varphi}](\boldsymbol{x}) = \int_{\Gamma} \mathbf{D}(\boldsymbol{x}, \boldsymbol{y}) \boldsymbol{\varphi}(\boldsymbol{y}) ds_{\boldsymbol{y}}, \quad \boldsymbol{x} \notin \Gamma, \quad (13)$$

where the kernel is given by

$$\mathbf{D}(\boldsymbol{x}, \boldsymbol{y}) = (\mathcal{T}_{\boldsymbol{y}} \mathbf{G}(\boldsymbol{x}, \boldsymbol{y}))^\top$$

with  $\mathcal{T}_{\boldsymbol{y}}$  the traction operator acting on the variable  $\boldsymbol{y}$ . The corresponding boundary operator of double layer potential  $D$  is

$$\mathcal{D}[\boldsymbol{\varphi}](\boldsymbol{x}) = \int_{\Gamma} \mathbf{D}(\boldsymbol{x}, \boldsymbol{y}) \boldsymbol{\varphi}(\boldsymbol{y}) ds_{\boldsymbol{y}}, \quad \boldsymbol{x} \in \Gamma. \quad (14)$$

The adjoint of double layer boundary operator is defined by

$$\mathcal{D}'[\boldsymbol{\varphi}](\boldsymbol{x}) = \int_{\Gamma} \boldsymbol{\Sigma}(\boldsymbol{x}, \boldsymbol{y}) \boldsymbol{\varphi}(\boldsymbol{y}) ds_{\boldsymbol{y}}, \quad \boldsymbol{x} \in \Gamma, \quad (15)$$

with

$$\boldsymbol{\Sigma}(\boldsymbol{x}, \boldsymbol{y}) = \mathcal{T}_{\boldsymbol{x}} \mathbf{G}(\boldsymbol{x}, \boldsymbol{y}).$$

Note that both the double layer boundary operator and its adjoint are defined in the sense of Cauchy principal value. Similar to the acoustic case [9], the double layer potential  $D[\boldsymbol{\varphi}](\boldsymbol{x})$  and the traction of single layer potential  $S[\boldsymbol{\varphi}](\boldsymbol{x})$  will produce a jump when  $\boldsymbol{x}$  approaches the boundary  $\Gamma$  [17], i.e.

$$\begin{aligned} \lim_{\epsilon \rightarrow 0^+} D[\boldsymbol{\varphi}](\boldsymbol{x} \pm \epsilon \boldsymbol{n}) &= \pm \frac{1}{2} \boldsymbol{\varphi}(\boldsymbol{x}) + \mathcal{D}[\boldsymbol{\varphi}](\boldsymbol{x}), \\ \lim_{\epsilon \rightarrow 0^+} \mathcal{T}_{\boldsymbol{x}} S[\boldsymbol{\varphi}](\boldsymbol{x} \pm \epsilon \boldsymbol{n}) &= \mp \frac{1}{2} \boldsymbol{\varphi}(\boldsymbol{x}) + \mathcal{D}'[\boldsymbol{\varphi}](\boldsymbol{x}), \end{aligned} \quad (16)$$

where the unit normal vector  $\boldsymbol{n}$  is towards the unbounded side of  $\Gamma$ . Note that (16) holds except for the corner points as the limit depends on the opening angle  $\theta_c$  [2]. Based on (16), we can formulate the boundary integral equations for elastic scattering in both Dirichlet and Neumann cases.

**3.1. Dirichlet problems.** For rigid boundary  $\Gamma$ , the solution  $\boldsymbol{u}_D^{sc}$  to equation (2) can be represented as the double layer potential

$$\boldsymbol{u}_D^{sc}(\boldsymbol{x}) = D[\boldsymbol{\varphi}_D](\boldsymbol{x}) = \int_{\Gamma} (\mathcal{T}_{\boldsymbol{y}} \mathbf{G}(\boldsymbol{x}, \boldsymbol{y}))^\top \boldsymbol{\varphi}_D(\boldsymbol{y}) ds_{\boldsymbol{y}}, \quad \boldsymbol{x} \in \Omega, \quad (17)$$

which results in a second kind boundary integral equation for the unknown vector function  $\boldsymbol{\varphi}_D$

$$\left( \pm \frac{1}{2} \mathcal{I} + \mathcal{D} \right) \boldsymbol{\varphi}_D = -\boldsymbol{u}^{inc}, \quad \boldsymbol{x} \in \Gamma. \quad (18)$$

Here we take ‘+’ for the exterior problem and ‘-’ for the interior problem.

**Remark 3.1.** Under the assumption that the wavenumber  $k_p$  and  $k_s$  are not the eigenvalue of the interior Dirichlet problems or Neumann problems, there exists a unique solution for the boundary integral equation (18) in both interior and exterior cases [21].

**Remark 3.2.** For the exterior problems, one can also follow a similar approach in [9] to formulate a combined layer potential to represent the scattered field

$$\mathbf{u}_D^{sc}(\mathbf{x}) = (D - iS)[\varphi_D](\mathbf{x}) = \int_{\Gamma} ((\mathcal{T}_y \mathbf{G})^\top - i\mathbf{G})(\mathbf{x}, \mathbf{y}) \varphi_D(\mathbf{y}) ds_{\mathbf{y}}, \quad \mathbf{x} \in \Omega, \quad (19)$$

which leads to the boundary integral equation

$$\left( \frac{1}{2} \mathcal{I} + \mathcal{D} - i\mathcal{S} \right) \varphi_D = -\mathbf{u}^{inc}, \quad \mathbf{x} \in \Gamma. \quad (20)$$

It is resonance free for any positive wavenumber  $k_p$  and  $k_s$ .

**3.2. Neumann problems.** For the Neumann problem (4), the scattered field  $\mathbf{u}_N^{sc}$  can be represented by the single layer potential

$$\mathbf{u}_N^{sc}(\mathbf{x}) = S[\varphi_N](\mathbf{x}) = \int_{\Gamma} \mathbf{G}(\mathbf{x}, \mathbf{y}) \varphi_N(\mathbf{y}) ds_{\mathbf{y}}, \quad \mathbf{x} \in \Omega, \quad (21)$$

where the unknown vector function  $\varphi_N$  satisfies the second kind boundary integral equation

$$\left( \mp \frac{1}{2} \mathcal{I} + \mathcal{D}' \right) \varphi_N = -\mathcal{T} \mathbf{u}^{inc}, \quad \mathbf{x} \in \Gamma. \quad (22)$$

Here we take ‘-’ for the exterior problem and ‘+’ for the interior problem.

**Remark 3.3.** Similar to the Dirichlet problem, there exists a unique solution to the boundary integral equation (22) when  $k_p$  and  $k_s$  are not the interior eigenvalues.

**Remark 3.4.** One can also represent the scattered field  $\mathbf{u}_N^{sc}$  for the exterior Neumann problem by the combined layer potential as (19), so that the resulted boundary integral equation is resonance free for all the exterior Neumann problems. Nevertheless, it will introduce the hyper-singular boundary operator, which transforms the equation from second kind and thereby difficult to discretize. Discussion on the hyper-singular boundary integral formulation can be found in [3].

**3.3. Kernel splitting of the boundary operators.** In order to construct a high-order numerical method for the boundary integral equations (18) and (22), we need to analyze the singularities of kernels in the single and double layer boundary operators. To simplify the presentation, let us denote  $\mathbf{r} = \mathbf{x} - \mathbf{y}$ ,  $r = |\mathbf{x} - \mathbf{y}|$ ,  $\mathbf{r}^\perp = (-(x_2 - y_2), (x_1 - y_1))^\top$ , and  $\otimes$  the outer product of two vectors. We also set

$$\mathbf{L} = \begin{pmatrix} 0 & 1 \\ -1 & 0 \end{pmatrix}. \quad (23)$$

Based on the identity [28, §10.6.6]

$$\frac{d}{dz} \left( \frac{H_n^{(1)}(z)}{z^n} \right) = -\frac{H_{n+1}^{(1)}(z)}{z^n}, \quad (24)$$

it yields

$$\begin{aligned} \partial_{x_i} H_0^{(1)}(kr) &= -k H_1^{(1)}(kr) \frac{x_i - y_i}{r}, \\ \partial_{x_j} \partial_{x_i} H_0^{(1)}(kr) &= k^2 H_2^{(1)}(kr) \frac{(x_i - y_i)(x_j - y_j)}{r^2} - k H_1^{(1)}(kr) \frac{\delta_{ij}}{r}, \\ \partial_{x_l} \partial_{x_j} \partial_{x_i} H_0^{(1)}(kr) &= -k^3 H_3^{(1)}(kr) \frac{(x_l - y_l)(x_i - y_i)(x_j - y_j)}{r^3} \\ &\quad + k^2 H_2^{(1)}(kr) \frac{\delta_{ij}(x_l - y_l) + \delta_{il}(x_j - y_j) + \delta_{jl}(x_i - y_i)}{r^2}, \end{aligned} \quad (25)$$

with  $i, j, l = 1$  or  $2$ . Thus, we get the explicit form for the kernel of single layer potential

$$\begin{aligned} \mathbf{G}(\mathbf{x}, \mathbf{y}) = & \frac{i}{4\mu} \left\{ H_0^{(1)}(k_s r) \mathbf{I} + \frac{1}{k_s^2} \left( k_s^2 H_2^{(1)}(k_s r) - k_p^2 H_2^{(1)}(k_p r) \right) \frac{\mathbf{r} \otimes \mathbf{r}}{r^2} \right. \\ & \left. + \frac{1}{k_s^2} \left( -k_s H_1^{(1)}(k_s r) + k_p H_1^{(1)}(k_p r) \right) \frac{\mathbf{I}}{r} \right\}. \end{aligned} \quad (26)$$

When  $z \rightarrow 0$ , it holds the following asymptotic properties for the Hankel functions [28]

$$\begin{aligned} H_0^{(1)}(z) &= J_0(z) + i \left\{ \frac{2}{\pi} \left( \ln \left( \frac{z}{2} \right) + \gamma \right) J_0(z) + O(z^2) \right\}, \\ H_1^{(1)}(z) &= J_1(z) + i \left\{ \frac{2}{\pi} \left( -\frac{1}{z} + \ln \left( \frac{z}{2} \right) \right) J_1(z) - \frac{z}{2\pi} (1 - 2\gamma) + O(z^3) \right\}, \\ H_2^{(1)}(z) &= J_2(z) + i \left\{ -\frac{4}{\pi} \frac{1}{z^2} - \frac{1}{\pi} + \frac{2}{\pi} \ln \left( \frac{z}{2} \right) J_2(z) - \frac{z^2}{4\pi} \left( \frac{3}{4} - \gamma \right) + O(z^4) \right\}, \\ H_3^{(1)}(z) &= J_3(z) + i \left\{ -\frac{8}{\pi} \left( \frac{2}{z^3} + \frac{1}{4z} + \frac{z}{32} \right) + \frac{2}{\pi} \ln \left( \frac{z}{2} \right) J_3(z) + O(z^3) \right\}, \end{aligned} \quad (27)$$

where  $\gamma$  is the Euler's constant and

$$J_0(z) \sim 1 + O(z^2), \quad J_1(z) \sim \frac{z}{2} + O(z^3), \quad J_2(z) \sim \frac{z^2}{8} + O(z^4), \quad J_3(z) \sim O(z^3). \quad (28)$$

Note that all the remainders in equations (27) and (28) are analytic with respect to  $z \in \mathbb{C}$ . We then obtain the asymptotic formula of  $\mathbf{G}(\mathbf{x}, \mathbf{y})$  as  $r \rightarrow 0$

$$\mathbf{G}(\mathbf{x}, \mathbf{y}) = \frac{1}{4\pi\mu} \left( -\frac{\lambda + 3\mu}{\lambda + 2\mu} \ln(r) \mathbf{I} + \frac{\lambda + \mu}{\lambda + 2\mu} \frac{\mathbf{r} \otimes \mathbf{r}}{r^2} \right) + O(1) + O(r^2 \ln r), \quad (29)$$

where the leading term is exactly  $\mathbf{E}(\mathbf{x}, \mathbf{y})$  for the Lamé equation. This explains that the single layer potential  $S$  is continuous across the boundary and the corresponding boundary operator is compact. However, equation (29) is not convenient for high-order discretization, we need another way to decompose  $\mathbf{G}$ .

**Lemma 3.5.** *It holds the decomposition that*

$$\mathbf{G}(\mathbf{x}, \mathbf{y}) = -\frac{2}{\pi} \ln(r) \text{Im}(\mathbf{G}(\mathbf{x}, \mathbf{y})) + \mathbf{R}_{\mathbf{G}}(\mathbf{x}, \mathbf{y}), \quad (30)$$

where  $\text{Im}(\mathbf{G}(\mathbf{x}, \mathbf{y}))$  is the imaginary part of  $\mathbf{G}(\mathbf{x}, \mathbf{y})$ . Both  $\text{Im}(\mathbf{G}(\mathbf{x}, \mathbf{y}))$  and the remainder  $\mathbf{R}_{\mathbf{G}}(\mathbf{x}, \mathbf{y})$  are analytic on  $\Gamma$  if  $\Gamma$  is smooth.

It is obtained by the asymptotic expansions (27) and the identity that  $H_n^{(1)}(z) = J_n(z) + iY_n(z)$ . When  $\mathbf{x} \rightarrow \mathbf{y}$  on  $\Gamma$ , we can explicitly obtain

$$\begin{aligned} \mathbf{R}_{\mathbf{G}}(\mathbf{x}, \mathbf{y}) \rightarrow & \frac{i}{4\mu} \left\{ \left( 1 + \frac{2i}{\pi} \left( \ln \left( \frac{k_s}{2} \right) + \gamma \right) \right) \mathbf{I} - \frac{1}{k_s^2} \frac{i}{\pi} (k_s^2 - k_p^2) \mathbf{M} \right. \\ & + \frac{1}{k_s^2} \left( -k_s^2 \left( \frac{1}{2} + i \left( \frac{1}{\pi} \ln \left( \frac{k_s}{2} \right) - \frac{1}{2\pi} (1 - 2\gamma) \right) \right) \right. \\ & \left. \left. + k_p^2 \left( \frac{1}{2} + i \left( \frac{1}{\pi} \ln \left( \frac{k_p}{2} \right) - \frac{1}{2\pi} (1 - 2\gamma) \right) \right) \right) \mathbf{I} \right\}, \end{aligned} \quad (31)$$

where  $\mathbf{M} = \lim_{\mathbf{x} \rightarrow \mathbf{y}} \frac{\mathbf{r} \otimes \mathbf{r}}{r^2}$ , which can be easily evaluated once the parametrization of  $\Gamma$  is given.

Similarly, by making use of equation (24), the kernel for the double layer boundary operator can be decomposed as follows.

**Theorem 3.6.** *It holds the decomposition that*

$$\mathbf{D}(\mathbf{x}, \mathbf{y}) = (\mathcal{T}_{\mathbf{y}}\mathbf{G}(\mathbf{x}, \mathbf{y}))^\top = (\mathcal{T}_{\mathbf{y}}\mathbf{E}(\mathbf{x}, \mathbf{y}))^\top + \ln(r)\mathbf{F}_{\mathbf{y}}(\mathbf{x}, \mathbf{y}) + \mathbf{R}_{\mathbf{D}}(\mathbf{x}, \mathbf{y}), \quad (32)$$

where

$$\begin{aligned} \mathcal{T}_{\mathbf{y}}\mathbf{E}(\mathbf{x}, \mathbf{y}) &= \frac{\mathbf{n}(\mathbf{y}) \cdot \mathbf{r}}{2\pi r^2} \mathbf{I} - \frac{\mu}{\lambda + 2\mu} \frac{\boldsymbol{\tau}(\mathbf{y}) \cdot \mathbf{r}}{2\pi r^2} \mathbf{L} \\ &\quad - \frac{\lambda + \mu}{\lambda + 2\mu} \left( -\frac{(\mathbf{n}(\mathbf{y}) \cdot \mathbf{r})\mathbf{r} \otimes \mathbf{r}}{\pi r^4} + \frac{(\mathbf{n}(\mathbf{y}) \cdot \mathbf{r})}{2\pi r^2} \mathbf{I} \right), \end{aligned} \quad (33)$$

$$\mathbf{F}_{\mathbf{y}}(\mathbf{x}, \mathbf{y}) = -\frac{2}{\pi} \operatorname{Im} \left\{ (\mathcal{T}_{\mathbf{y}}\mathbf{G}(\mathbf{x}, \mathbf{y}))^\top \right\}, \quad (34)$$

and  $\mathbf{R}_{\mathbf{D}}(\mathbf{x}, \mathbf{y}) \rightarrow 0$  when  $\mathbf{x} \rightarrow \mathbf{y}$ . If the boundary  $\Gamma$  is smooth, both  $\mathbf{F}_{\mathbf{y}}(\mathbf{x}, \mathbf{y})$  and the remainder term  $\mathbf{R}_{\mathbf{D}}(\mathbf{x}, \mathbf{y})$  in (32) are analytic on  $\Gamma$ .

**Remark 3.7.** Here  $(\mathcal{T}_{\mathbf{y}}\mathbf{E}(\mathbf{x}, \mathbf{y}))^\top$  is exactly the kernel of double layer potential of Lamé equation. The second term in  $(\mathcal{T}_{\mathbf{y}}\mathbf{E}(\mathbf{x}, \mathbf{y}))^\top$  is of order  $O(r^{-1})$  as  $r = |\mathbf{x} - \mathbf{y}| \rightarrow 0$ , which makes the boundary integral exist in the sense of Cauchy principal value [17].

*Proof.* By equation (24) and the definition of traction operator  $\mathcal{T}$  in (3), we have

$$\begin{aligned} \mathcal{T}_{\mathbf{y}}\mathbf{G}(\mathbf{x}, \mathbf{y}) &= \frac{i}{4} \left\{ \frac{k_s H_1^{(1)}(k_s r)}{r} \mathbf{L}_1(\mathbf{x}, \mathbf{y}) + \frac{\lambda}{\lambda + 2\mu} \frac{k_p H_1^{(1)}(k_p r)}{r} \mathbf{L}_2(\mathbf{x}, \mathbf{y}) \right. \\ &\quad + \frac{2}{k_s^2} \left( \frac{(k_s^3 H_3^{(1)}(k_s r) - k_p^3 H_3^{(1)}(k_p r))}{r^3} \mathbf{L}_3(\mathbf{x}, \mathbf{y}) \right. \\ &\quad \left. \left. - \frac{(k_s^2 H_2^{(1)}(k_s r) - k_p^2 H_2^{(1)}(k_p r))}{r^2} \mathbf{L}_4(\mathbf{x}, \mathbf{y}) \right) \right\}, \end{aligned} \quad (35)$$

where

$$\begin{aligned} \mathbf{L}_1(\mathbf{x}, \mathbf{y}) &= 2(\mathbf{n}(\mathbf{y}) \cdot \mathbf{r})\mathbf{I} - \boldsymbol{\tau}(\mathbf{y}) \otimes \mathbf{r}^\perp, \quad \mathbf{L}_2(\mathbf{x}, \mathbf{y}) = \mathbf{n}(\mathbf{y}) \otimes \mathbf{r}, \\ \mathbf{L}_3(\mathbf{x}, \mathbf{y}) &= (\mathbf{n}(\mathbf{y}) \cdot \mathbf{r})\mathbf{r} \otimes \mathbf{r}, \quad \mathbf{L}_4(\mathbf{x}, \mathbf{y}) = (\mathbf{n}(\mathbf{y}) \cdot \mathbf{r})\mathbf{I} + \mathbf{n}(\mathbf{y}) \otimes \mathbf{r} + \mathbf{r} \otimes \mathbf{n}(\mathbf{y}). \end{aligned} \quad (36)$$

Using the expansion (27), the asymptotic expansion for the double layer boundary operator can be rewritten as

$$\begin{aligned} \mathcal{T}_{\mathbf{y}}\mathbf{G}(\mathbf{x}, \mathbf{y}) &= \frac{\mathbf{L}_1(\mathbf{x}, \mathbf{y})}{2\pi r^2} - k_s \ln(r) J_1(k_s r) \frac{\mathbf{L}_1(\mathbf{x}, \mathbf{y})}{2\pi r} \\ &\quad + \frac{\lambda}{\lambda + 2\mu} \frac{\mathbf{L}_2(\mathbf{x}, \mathbf{y})}{2\pi r^2} - \frac{\lambda}{\lambda + 2\mu} \frac{k_p \ln(r) J_1(k_p r)}{2\pi r} \mathbf{L}_2(\mathbf{x}, \mathbf{y}) \\ &\quad - \frac{2}{k_s^2} \left\{ - (k_s^2 - k_p^2) \frac{\mathbf{L}_3(\mathbf{x}, \mathbf{y})}{2\pi r^4} + \frac{k_s^4 - k_p^4}{8} \frac{\mathbf{L}_3(\mathbf{x}, \mathbf{y})}{2\pi r^2} \right\} \\ &\quad - \frac{2}{k_s^2} (k_s^3 \ln(r) J_3(k_s r) - k_p^3 \ln(r) J_3(k_p r)) \frac{\mathbf{L}_3(\mathbf{x}, \mathbf{y})}{2\pi r^3} \\ &\quad - \frac{(k_s^2 - k_p^2)}{k_s^2} \frac{\mathbf{L}_4(\mathbf{x}, \mathbf{y})}{2\pi r^2} + \frac{2}{k_s^2} (k_s^2 \ln(r) J_2(k_s r) - k_p^2 \ln(r) J_2(k_p r)) \frac{\mathbf{L}_4(\mathbf{x}, \mathbf{y})}{2\pi r^2} \\ &\quad + O(r). \end{aligned} \quad (37)$$



Merging the logarithmic singular part and using the fact that

$$\mathbf{r} = (\mathbf{n}(\mathbf{y}) \cdot \mathbf{r})\mathbf{n}(\mathbf{y}) + (\boldsymbol{\tau}(\mathbf{y}) \cdot \mathbf{r})\boldsymbol{\tau}(\mathbf{y}), \quad \mathbf{r}^\perp = -(\boldsymbol{\tau}(\mathbf{y}) \cdot \mathbf{r})\mathbf{n}(\mathbf{y}) + (\mathbf{n}(\mathbf{y}) \cdot \mathbf{r})\boldsymbol{\tau}(\mathbf{y}), \quad (38)$$

$$\mathbf{I} = \mathbf{n}(\mathbf{y}) \otimes \mathbf{n}(\mathbf{y}) + \boldsymbol{\tau}(\mathbf{y}) \otimes \boldsymbol{\tau}(\mathbf{y}), \quad \mathbf{L} = \mathbf{n}(\mathbf{y}) \otimes \boldsymbol{\tau}(\mathbf{y}) - \boldsymbol{\tau}(\mathbf{y}) \otimes \mathbf{n}(\mathbf{y}), \quad (39)$$

where  $\mathbf{L}$  is defined in (23), we obtain the decomposition (32).  $\square$

One can analogously derive the asymptotic expansion for the kernel of the adjoint of the double layer boundary operator  $\mathcal{D}'$ .

**Corollary 3.8.** *It holds the decomposition that*

$$\boldsymbol{\Sigma}(\mathbf{x}, \mathbf{y}) = \mathcal{T}_x \mathbf{G}(\mathbf{x}, \mathbf{y}) = \mathcal{T}_x \mathbf{E}(\mathbf{x}, \mathbf{y}) + \ln(r)\mathbf{F}_x(\mathbf{x}, \mathbf{y}) + \mathbf{R}_\Sigma(\mathbf{x}, \mathbf{y}), \quad (40)$$

with

$$\begin{aligned} \mathcal{T}_x \mathbf{E}(\mathbf{x}, \mathbf{y}) &= -\frac{\mathbf{n}(\mathbf{x}) \cdot \mathbf{r}}{2\pi r^2} \mathbf{I} + \frac{\mu}{\lambda + 2\mu} \frac{\boldsymbol{\tau}(\mathbf{x}) \cdot \mathbf{r}}{2\pi r^2} \mathbf{L} \\ &+ \frac{\lambda + \mu}{\lambda + 2\mu} \left( -\frac{(\mathbf{n}(\mathbf{x}) \cdot \mathbf{r})\mathbf{r} \times \mathbf{r}}{\pi r^4} + \frac{(\mathbf{n}(\mathbf{x}) \cdot \mathbf{r})}{2\pi r^2} \mathbf{I} \right), \end{aligned} \quad (41)$$

$$\mathbf{F}_x(\mathbf{x}, \mathbf{y}) = -\frac{2}{\pi} \operatorname{Im} \{ \mathcal{T}_x \mathbf{G}(\mathbf{x}, \mathbf{y}) \}, \quad (42)$$

and  $\mathbf{R}_\Sigma(\mathbf{x}, \mathbf{y}) \rightarrow 0$  when  $\mathbf{x} \rightarrow \mathbf{y}$ . Both  $\mathbf{F}_x(\mathbf{x}, \mathbf{y})$  and  $\mathbf{R}_\Sigma(\mathbf{x}, \mathbf{y})$  are analytic on  $\Gamma$  if  $\Gamma$  is smooth.

We conclude from (29), (32) and (40) that the principal parts of the kernel functions of elastic wave equation are the kernel functions of Lamé equation, which is similar to the relation between Helmholtz equation and Laplace equation. The difference is that the double layer boundary operator and its adjoint in elastic equations have Cauchy singularity even after the extraction of identity operator. Conventional quadrature method based on weakly singular integrals fails to give a high-order discretization. In the next section, we will make use of the kernel splitting results (30), (32) and (40) to obtain a high-order Nyström discretization for the singular boundary operators.

#### 4. NUMERICAL DISCRETIZATION

Nyström discretization is a commonly used numerical approach for boundary integral equations [2, 19]. For smooth geometries, Nyström method based on trigonometric interpolation seems to be the most effective way to discretize singular integrals and converges exponentially fast [11]. However, its effectiveness diminishes in geometries with corners, where a large number of Fourier modes are required to fully resolve corner singularities. Here we choose to discretize the boundary integral equation based on the piecewise polynomial interpolation. In particular, we make use of the composite Gauss-Legendre nodes and the analytical singular integrals to discretize the kernels given by equations (29), (32), and (40). We will show that the singular quadrature based on such kernel-splitting method with uniform partition can achieve 15-digits of accuracy or more on the smooth geometries. Nevertheless, these digits can be easily lost in the cornered domains due to the limitations of uniform mesh in fully resolving the corner singularities. In order to construct a high-order and efficient numerical method for the elastic scattering problems from cornered domains, we adopt a graded mesh near the corners to discretize the boundary. This approach effectively resolves corner singularities while concomitantly enlarging the discretized matrix and escalating the condition number. Directly inverting the resulted linear system is numerically unstable due to the round-off errors of small weights [6]. Therefore, a method is required to maintain the well-conditioning of the discretized linear system while keeping computational costs relatively low. For that purpose, the recursively compressed inverse preconditioning method (RCIP) [15] is employed for the discretized scattering problems from cornered domains.

In the following, we will give the details of the Nyström method for the elastic scattering using the composite Gauss-Legendre quadrature and analytical singular integrals, and then briefly describe the RCIP method.

**4.1. Discretization of singular integrals.** Assume that the piecewise smooth boundary  $\Gamma$  is parameterized by

$$\mathbf{x}(s) = (x_1(s), x_2(s)), \quad s \in [0, L].$$

We first divide each smooth component of  $\Gamma$  into  $N$  uniform panels, where  $N$  can be different for each component. We call the uniform mesh as the coarse mesh. Due to the corner singularity, we apply the non-uniform discretization in the neighborhood of each corner point using graded mesh. More specifically, assume the first panel is  $[0, 1]$  with 0 corresponding to the corner point, we subdivide it into  $n_{sub} + 1$  smaller panels as  $[0, (1/2)^{n_{sub}}] \cup [(1/2)^{n_{sub}}, (1/2)^{n_{sub}-1}] \cup \dots \cup [1/2, 1]$ . See Figure 1 for an illustration of the coarse and refined meshes.

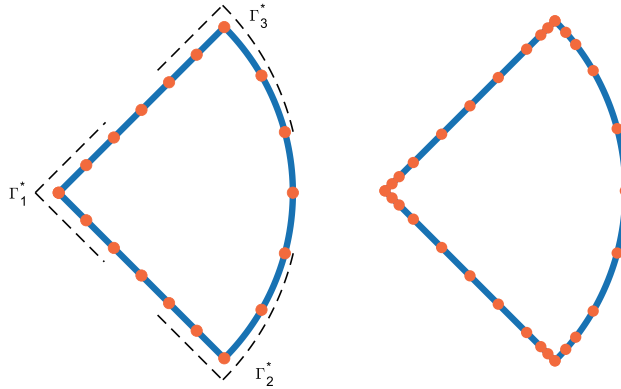


FIGURE 1. Discretization of a piecewise smooth boundary  $\Gamma$ . On the left is a coarse mesh, where each smooth component of  $\Gamma$  is divided equally into  $N$  panels. For each corner point, we use the nearest four coarse panels to represent its neighborhood. On the right is the refined mesh obtained by dyadically subdividing the panels adjacent to the corners.

Denote  $\Gamma_i$  the  $i$ th panel,  $i = 1, 2, \dots, N$ . For the panel  $\Gamma_i$ , we further discretize it by Gauss-Legendre quadrature with nodes  $s_{ij}$  and weights  $w_{ij}$ ,  $j = 0, 1, \dots, n-1$ . Here denote the corresponding points on the panel  $\Gamma_i$  by  $\mathbf{x}_{ij} = \mathbf{x}(s_{ij})$  or  $\mathbf{y}_{ij} = \mathbf{y}(s_{ij})$ . Given  $\mathbf{x} \in \Gamma_l$ ,  $l = 1, 2, \dots, N$ , consider the boundary integral in the form of

$$\mathcal{K}_i[\boldsymbol{\varphi}](\mathbf{x}) = \int_{\Gamma_i} \mathbf{K}(\mathbf{x}, \mathbf{y}) \boldsymbol{\varphi}(\mathbf{y}) ds_{\mathbf{y}}, \quad \mathbf{x} \in \Gamma_l, \quad (43)$$

where  $\mathbf{K}(\mathbf{x}, \mathbf{y})$  is the kernel function with singularity at  $\mathbf{x} = \mathbf{y}$ . When  $\Gamma_l$  and  $\Gamma_i$  are distant from each other, the usual Nyström discretization reads

$$\int_{\Gamma_i} \mathbf{K}(\mathbf{x}, \mathbf{y}) \boldsymbol{\varphi}(\mathbf{y}) ds_{\mathbf{y}} \approx \sum_{j=0}^{n-1} \mathbf{K}(\mathbf{x}, \mathbf{y}_{ij}) \boldsymbol{\varphi}(\mathbf{y}_{ij}) w_{ij} J_i(s_{ij}) \quad (44)$$

where  $J_i(s)$  is the Jacobian on panel  $\Gamma_i$ . It will achieve high-order accuracy except for adjacent or self-interacting panels of  $\Gamma_l$ , i.e.  $l = i-1, i, i+1$ , due to the singularity of the kernel function. One remedy is to switch the quadrature to the generalized Gaussian quadrature scheme [7]. It is accurate for logarithmic singularity but less effective for Cauchy singularity. In this paper, we employ the decomposition (30), (32), and (40) to split each kernel into a combination of an analytically integrable singular part and a smooth non-singular part. For the singular part, one can integrate it by the

analytical formula, while for the smooth part, the usual Gaussian quadrature (44) will give a high-order accuracy. More specifically, we first transform the integral on  $\Gamma_i$  to  $[-1, 1]$  by a suitable change of variables. Substituting the parametrization  $\mathbf{x}(t)$  and  $\mathbf{y}(s)$  into the expressions (30), (32), and (40), one can convert the kernel functions into

$$\mathbf{K}(\mathbf{x}(t), \mathbf{y}(s)) = \ln(|t-s|)\mathbf{K}_1(t, s) + \frac{1}{t-s}\mathbf{K}_2(t, s) + \mathbf{K}_3(t, s), \quad (45)$$

which swaps the singularity from  $\mathbf{x}$  and  $\mathbf{y}$  to the parameters  $t$  and  $s$ . Besides,  $\mathbf{K}_1, \mathbf{K}_2$  and  $\mathbf{K}_3$  are all analytical functions on  $\Gamma_i$ . Taking (32) as an example, the kernel  $\mathbf{D}(\mathbf{x}, \mathbf{y})$  can be rewritten as

$$\begin{aligned} & \mathbf{D}(\mathbf{x}(t), \mathbf{y}(s)) \\ &= \ln(|t-s|)\mathbf{F}_\mathbf{y}(\mathbf{x}, \mathbf{y}) + \frac{1}{t-s} \left( -\frac{(t-s)\mu}{\lambda+2\mu} \frac{\boldsymbol{\tau}(\mathbf{x}) \cdot \mathbf{r}}{2\pi r^2} \mathbf{L}^\top \right) \\ &+ \left( (\ln(r) - \ln(|t-s|))\mathbf{F}_\mathbf{y}(\mathbf{x}, \mathbf{y}) + (\mathcal{T}_\mathbf{y}\mathbf{E}(\mathbf{x}, \mathbf{y}))^\top + \frac{\mu}{\lambda+2\mu} \frac{\boldsymbol{\tau}(\mathbf{x}) \cdot \mathbf{r}}{2\pi r^2} \mathbf{L}^\top + \mathbf{R}_\mathbf{D}(\mathbf{x}, \mathbf{y}) \right). \end{aligned} \quad (46)$$

**Remark 4.1.** *Theoretically, when  $\mathbf{x} \neq \mathbf{y}$ , the value of  $\mathbf{R}_\mathbf{G}$ ,  $\mathbf{R}_\mathbf{D}$ , and  $\mathbf{R}_\Sigma$  can be obtained by taking the difference of the left and right hand sides of equations (30), (32) and (40), respectively. However, in the numerical implementation, when  $\mathbf{x}$  is very close to  $\mathbf{y}$ , one should switch to the asymptotic expansions of  $\mathbf{R}_\mathbf{G}$ ,  $\mathbf{R}_\mathbf{D}$ , and  $\mathbf{R}_\Sigma$  based on equations (27) and (28) to avoid numerical round-off errors.*

Then the integral (43) can be approximated by

$$\begin{aligned} & \int_{\Gamma_i} \mathbf{K}(\mathbf{x}, \mathbf{y})\boldsymbol{\varphi}(\mathbf{y})ds(\mathbf{y}) \\ &= \int_{-1}^1 \left[ \ln(|t-s|)\mathbf{K}_1(t, s) + \frac{1}{t-s}\mathbf{K}_2(t, s) + \mathbf{K}_3(t, s) \right] \boldsymbol{\varphi}(s)J_i(s)ds \\ &\approx \int_{-1}^1 \left[ \ln(|t-s|) \sum_{j=0}^{n-1} c_{ij}P_j(s) + \frac{1}{t-s} \sum_{j=0}^{n-1} d_{ij}P_j(s) + \sum_{j=0}^{n-1} f_{ij}P_j(s) \right] ds \\ &= \sum_{j=0}^{n-1} \left( c_{ij} \int_{-1}^1 \ln(|t-s|)P_j(s)ds + d_{ij} \int_{-1}^1 \frac{1}{t-s}P_j(s)ds + f_{ij} \int_{-1}^1 P_j(s)ds \right) \end{aligned} \quad (47)$$

where  $P_j(s)$  is the Legendre polynomial of degree  $j$ ,  $c_{ij}, d_{ij}$ , and  $f_{ij}$  are the expansion coefficients of Legendre polynomials for  $\mathbf{K}_1\boldsymbol{\varphi}J_i, \mathbf{K}_2\boldsymbol{\varphi}J_i$  and  $\mathbf{K}_3\boldsymbol{\varphi}J_i$ . These coefficients can be obtained by using the  $n \times n$  interpolation matrix  $U = (u_{jk})$  that maps the value at the Gauss-Legendre nodes to the coefficients of  $P_j$ . In other words, it holds

$$c_{ij} = \sum_{k=0}^{n-1} u_{jk}[\mathbf{K}_1\boldsymbol{\varphi}J_i](s_{ik}), \quad d_{ij} = \sum_{k=0}^{n-1} u_{jk}[\mathbf{K}_2\boldsymbol{\varphi}J_i](s_{ik}), \quad f_{ij} = \sum_{k=0}^{n-1} u_{jk}[\mathbf{K}_3\boldsymbol{\varphi}J_i](s_{ik}). \quad (48)$$

Denote

$$L_j = \int_{-1}^1 \ln(|t-s|)P_j(s)ds, \quad C_j = \int_{-1}^1 \frac{1}{t-s}P_j(s)ds, \quad I_j = \int_{-1}^1 P_j(s)ds. \quad (49)$$

The value of  $I_j$  can be easily obtained by the orthogonality of Legendre polynomials. The evaluation of  $L_j$  and  $C_j$  will be discussed in the next subsection. Once they are calculated, by combining (48)

and (49), we can rewrite the integral (47) as

$$\begin{aligned}
\int_{\Gamma_i} \mathbf{K}(\mathbf{x}, \mathbf{y}) \boldsymbol{\varphi}(\mathbf{y}) ds(\mathbf{y}) &\approx \sum_{j=0}^{n-1} \left( \sum_{k=0}^{n-1} u_{jk} (L_j \mathbf{K}_1 \boldsymbol{\varphi} J_i + C_j \mathbf{K}_2 \boldsymbol{\varphi} J_i + I_j \mathbf{K}_3 \boldsymbol{\varphi} J_i) \right) \\
&= \sum_{k=0}^{n-1} \left[ \sum_{j=0}^{n-1} u_{jk} (L_j \mathbf{K}_1 + C_j \mathbf{K}_2 + I_j \mathbf{K}_3) \right] \boldsymbol{\varphi} J_i(s_{ik}) \\
&= \sum_{k=0}^{n-1} \tilde{w}_{ik} \boldsymbol{\varphi}(s_{ik}),
\end{aligned} \tag{50}$$

where  $\tilde{w}_{ik} = \sum_{j=0}^{n-1} u_{jk} (L_j \mathbf{K}_1 + C_j \mathbf{K}_2 + I_j \mathbf{K}_3) J_i$  can be taken as the modified singular quadrature weights for the integral (43). Note that they not only depend on the Jacobian  $J_i$  at  $s_{ik}$ , but also the target and source points  $\mathbf{x}(t)$  and  $\mathbf{y}(s)$ .

**4.2. Analytical singular integrals.** Through the discussion above, the discretization of singular integrals is transformed into the evaluation of (49). In this part, we focus on the computation of  $L_j$  and  $C_j$ ,  $j = 0, \dots, n-1$  and note that they only need to be computed once. It is worth mentioning that the singular integrals for monomials have been discussed in [14]. We proceed by evaluating  $C_j$  first, as the evaluation of  $L_j$  is based on  $C_j$ .

**4.2.1. Cauchy singular integrals.** For a fixed  $t \in \mathbb{R}$  and  $t \neq \pm 1$ , it holds

$$\begin{aligned}
C_0 &= \int_{-1}^1 \frac{1}{t-s} P_0(s) ds = -\ln \left| \frac{t-1}{t+1} \right|, \\
C_1 &= \int_{-1}^1 \frac{1}{t-s} P_1(s) ds = -2 + tC_0,
\end{aligned}$$

where the integral exists in the sense of Cauchy principal value when  $t \in (-1, 1)$ . For  $j \geq 2$ , we can make use of the recursive formula for Legendre polynomials

$$jP_j(s) = (2j-1)sP_{j-1}(s) - (j-1)P_{j-2}(s),$$

to obtain the recursion formula of  $C_j$ ,

$$jC_j = (2j-1)tC_{j-1} - (j-1)C_{j-2}.$$

**4.2.2. Logarithmic singular integrals.** We will make use of the Cauchy singular integral  $C_j$  to compute the logarithmic integral  $L_j$ . More specifically, it holds

$$\begin{aligned}
L_0 &= \int_{-1}^1 \ln |t-s| P_0(s) ds = (t+1) \ln |t+1| - (t-1) \ln |t-1| - 2, \\
L_1 &= \int_{-1}^1 \ln |t-s| P_1(s) ds = tL_0 - \left( \frac{(t+1)^2}{2} \ln |t+1| - \frac{(t-1)^2}{2} \ln |t-1| - t \right).
\end{aligned}$$

For  $j \geq 2$ , according to the formula

$$\frac{d(P_{j+1}(s) - P_{j-1}(s))}{ds} = (2j+1)P_j(s),$$

we have

$$\begin{aligned}
jL_j &= j \int_{-1}^1 \ln |t-s| P_j(s) ds \\
&= \begin{cases} -[L_j - L_{j-2}] + t[C_j - C_{j-2}] - (j-1)L_{j-2} + 2, & \text{if } j = 2, \\ -[L_j - L_{j-2}] + t[C_j - C_{j-2}] - (j-1)L_{j-2}, & \text{otherwise.} \end{cases}
\end{aligned}$$

It implies for  $j = 2$ ,

$$(j + 1)L_j = t[C_j - C_{j-2}] + 2,$$

and for  $j > 2$

$$(j + 1)L_j = -(j - 2)L_{j-2} + t[C_j - C_{j-2}].$$

Consequently, we are able to evaluate all the  $C_j$  and  $L_j$  for  $j = 0, 1, \dots, n-1$  based on these recursive formulas and therefore construct the modified singular quadrature in the Nyström discretization (44).

**4.3. Recursively compressed inverse preconditioning.** RCIP was proposed in [15] as a kernel-independent numerical algorithm used to solve the second kind boundary integral equations. Here we only give a brief introduction of RCIP, as the details are given in [15]. The main idea of RCIP is to use the interpolation matrix to construct an inverse preconditioner that transforms the information from fine grid to coarse grid, which leads to a linear system on the coarse mesh that is much easier to solve. The method is purely algebraic and independent of singular kernels.

Consider the integral equation of the second kind on the boundary  $\Gamma$  with some corner points,

$$(\mathcal{I} + \mathcal{K})\boldsymbol{\varphi}(x) = \mathbf{g}(x), \quad x \in \Gamma, \quad (51)$$

where  $\mathcal{K}$  is presumably a compact operator away from the corner. This is not mandatory in the numerical practice, as in the elastic scattering case, the double layer boundary operator and its adjoint are not compact even on the smooth boundaries [17]. According to the mesh generation illustrated by Figure 1, we denote the four coarse grid panels near each corner point by  $\Gamma_k^*$ ,  $k = 1, 2, \dots, M$ , where  $M$  is the number of corner points. We then split the operator into  $\mathcal{K} = \mathcal{K}^* + \mathcal{K}^o$ , where  $\mathcal{K}^*$  is the operator when the target point  $\mathbf{x}$  and source point  $\mathbf{y}$  are both at the same  $\Gamma_k^*$ . Thus the equation is formulated into the following linear system of equations on the coarse and fine meshes

$$(\mathbb{I}_{coa} + \mathbb{K}_{coa}^* + \mathbb{K}_{coa}^o)\boldsymbol{\varphi}_{coa} = \mathbf{g}_{coa}, \quad (52)$$

$$(\mathbb{I}_{fin} + \mathbb{K}_{fin}^* + \mathbb{K}_{fin}^o)\boldsymbol{\varphi}_{fin} = \mathbf{g}_{fin}. \quad (53)$$

Here  $\mathbb{I}$  is the identity matrix,  $\mathbb{K}^*$  and  $\mathbb{K}^o$  are square matrices,  $\{\boldsymbol{\varphi}_{coa}, \boldsymbol{\varphi}_{fin}\}$  and  $\{\mathbf{g}_{coa}, \mathbf{g}_{fin}\}$  are the discretized densities and incident waves on the coarse and fine meshes respectively.

Next, we introduce the prolongation matrix  $\mathbb{P}$ , which maps points on the coarse grid to points on the fine grid by Gauss-Legendre polynomial interpolation. It holds

$$\mathbf{g}_{fin} \approx \mathbb{P}\mathbf{g}_{coa}. \quad (54)$$

The weighted matrix  $\mathbb{P}_W = \mathbb{W}_{fin}\mathbb{P}\mathbb{W}_{coa}^{-1}$  also needs to be constructed, where  $\mathbb{W}_{coa}$  and  $\mathbb{W}_{fin}$  are two diagonal matrices whose diagonal elements are the integral weights on the coarse and fine meshes respectively. It also holds the property [15] that

$$\mathbb{K}_{fin}^o \approx \mathbb{P}\mathbb{K}_{coa}^o\mathbb{P}_W^T. \quad (55)$$

Let us introduce the substitution of variable

$$\boldsymbol{\varphi}_{fin} = (\mathbb{I}_{fin} + \mathbb{K}_{fin}^*)^{-1}\tilde{\boldsymbol{\varphi}}_{fin} = (\mathbb{I}_{fin} + \mathbb{K}_{fin}^*)^{-1}\mathbb{P}\tilde{\boldsymbol{\varphi}}_{coa}. \quad (56)$$

Substituting equation (56) into equation (53), and applying the weighted prolongation matrix  $\mathbb{P}_W$ , we obtain

$$(\mathbb{I}_{coa} + \mathbb{K}_{coa}^o\mathbb{P}_W^T(\mathbb{I}_{fin} + \mathbb{K}_{fin}^*)^{-1}\mathbb{P})\tilde{\boldsymbol{\varphi}}_{coa} = \mathbf{g}_{coa}, \quad (57)$$

where the equal sign is given up to a negligible numerical error. Denote  $\mathbb{R} = \mathbb{P}_W^T(\mathbb{I}_{fin} + \mathbb{K}_{fin}^*)^{-1}\mathbb{P}$  the compressed weighted inverse, which is complicated to evaluate directly but in practice can be evaluated through recursive operations [15].

Therefore, the problem of solving linear equations (53) on the fine grid is transformed into the equation (57) on the coarse grid, which not only improves the numerical stability, but also greatly

reduces the computational cost. Once equation (57) is solved, we can obtain the solution  $\hat{\varphi}_{coa}$  for the density function on the coarse grid via

$$\hat{\varphi}_{coa} = \mathbb{R}\tilde{\varphi}_{coa}. \quad (58)$$

Compared to  $\varphi_{coa}$  in (52),  $\hat{\varphi}_{coa}$  carries the information from the fine grid and is sufficient for the field evaluation away from the corner points. If the field near the corners is needed, one can also reconstruct  $\varphi_{fin}$  on  $\Gamma_k^*$  by a reverse recursion formula. More details can be found in [15].

**4.4. Convergence.** Analyzing the convergence of Nyström method in the presence of corners is typically challenging. The convergence analysis for discretizing the second kind boundary integral equation for Helmholtz equations in cornered domains can be found at [20]. However, the proof cannot be directly extended to the elastic equation due to the non-compactness of the boundary operator  $\mathcal{D}$  and  $\mathcal{D}'$  in equations (18) and (22). In case the boundary is smooth, as shown in [11], we have established the convergence of the Nyström discretization based on the Helmholtz decomposition and trigonometric interpolation. One of the key ingredients in the proof is to construct an appropriate regularizer for the boundary operator, thus converting the equation into the form of an invertible operator combined with a compact one. One might follow the same idea with a detailed spectral analysis for boundary operators near the corner to prove the convergence of the proposed method. In this paper, we mainly focus on the numerical discretization of the elastic boundary integral equations, deferring the convergence analysis to future research.

## 5. NUMERICAL EXPERIMENTS

In this section, we will test our algorithm by several numerical examples. The geometries used in the numerical tests are shown in Figure 2, namely, a circle, an ellipse, a droplet and a sector. Obviously, the droplet and the sector in Figures 2(C) and 2(D) are non-smooth with some corner points. The parametrizations for the circle and the ellipse are given by

$$\mathbf{x}(s) = \begin{cases} x_1 = 2\alpha \cos(s), \\ x_2 = 2\alpha \sin(s), \end{cases} \quad s \in [0, 2\pi], \quad (59)$$

with  $\alpha = 1$  for the circle (Figure 2(A)) and  $\alpha = 2$  for the ellipse (Figure 2(B)). The droplet is given by

$$\mathbf{x}(s) = \begin{cases} x_1 = \sin(\pi s)(\cos(\pi/2(s - 0.5))), \\ x_2 = \sin(\pi s)(\sin(\pi/2(s - 0.5))), \end{cases} \quad s \in [0, 1], \quad (60)$$

and the sector is parameterized as

$$\mathbf{x}(s) = (x_1(s), x_2(s)) = \begin{cases} (\beta s, -\beta k s), & s \in [0, 1], \\ (\cos(2\theta s - 3\theta), \sin(2\theta s - 3\theta)), & s \in [1, 2], \\ (-\beta s + 3\beta, -\beta k s + 3k\beta), & s \in [2, 3], \end{cases} \quad (61)$$

where  $k$  quantifies the opening of the sector with  $\beta = 1/\sqrt{1+k^2}$  and  $\theta = \arctan(k)$ .

We use *DND* to denote solving Dirichlet problems (18) by the double layer potential and *SNN* to denote solving Neumann problems (22) by the single layer potential, and use the subscripts *ex* and *in* to represent the exterior and interior problems, respectively. We set the Lamé parameters  $\lambda = 1$  and  $\mu = 2$ , the mass density  $\rho = 1$  and the angular frequency  $\omega = 3$  for all examples except example 3 where we test the performance of the solver at different wavenumbers. We choose  $n = 16$  for the number of Gauss-Legendre nodes placed in each panel during the discretization. To verify the accuracy, an artificial solution for the elastic equations is constructed by the point source technique. Namely, for the interior or exterior problems with domain  $\Omega$ , we can put a point source outside of  $\Omega$  and impose the exact boundary condition on  $\Gamma$ . When the boundary integral equation is solved correctly, the point source solution should be recovered in  $\Omega$  by the uniqueness theorem [21]. All the experiments are carried out by *MATLAB* on a laptop with an Intel CPU inside.

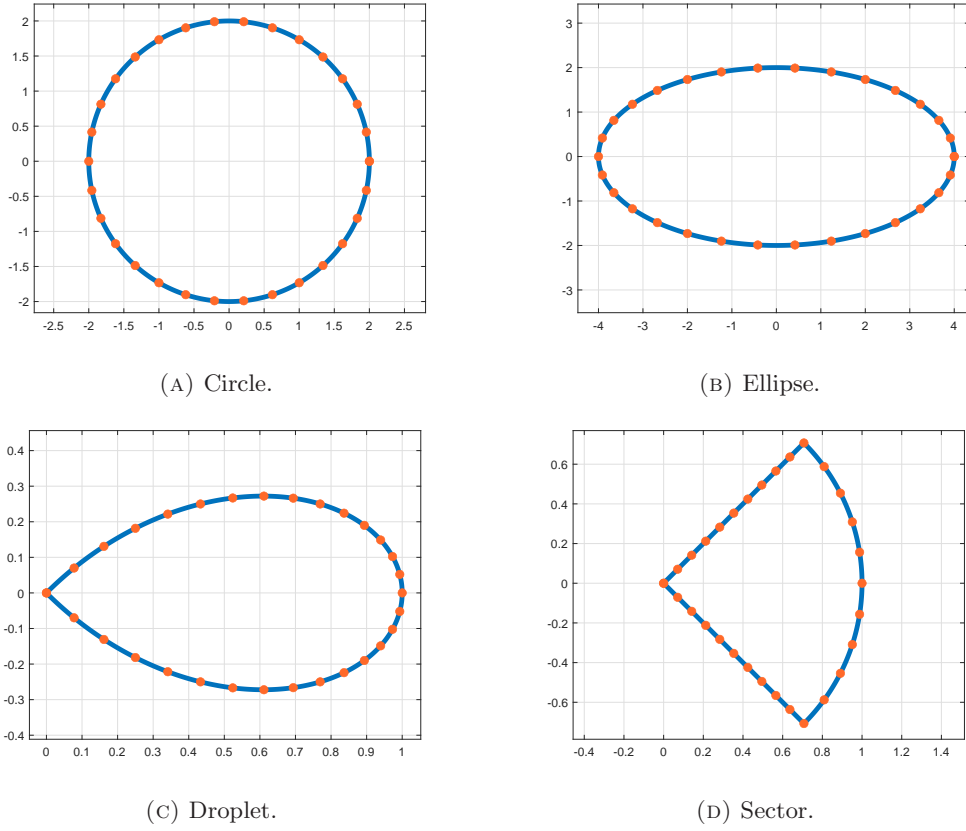


FIGURE 2. Four different geometries in the scattering of elastic waves.

**5.1. Example 1: Elastic scattering with uniform meshes.** In this example, We test the exterior problems from the four geometries using uniform discretization. The exact solution is constructed by using a point source located at  $\mathbf{y}_0 = (0.5, 0) \in \mathbb{R}^2 \setminus \Omega$  and we verify the field at  $\mathbf{x} = (12.1, 5.2)$ . The accuracy of the numerical results is shown in Table 1, where  $N$  is the number of panels and we check the errors for both the shear and compressional wave at each given  $N$ .

TABLE 1. Results of elastic scattering from four geometries by uniform discretization of the boundaries. Curves A, B, C and D represent the circle, ellipse, droplet and sector, respectively.

| N  | $DND_{ex}$ |          |          |          | $SNN_{ex}$ |          |          |          |
|----|------------|----------|----------|----------|------------|----------|----------|----------|
|    | Curve A    | Curve B  | Curve C  | Curve D  | Curve A    | Curve B  | Curve C  | Curve D  |
| 12 | 3.53E-17   | 5.22E-14 | 7.79E-06 | 2.96E-09 | 7.24E-17   | 9.94E-14 | 5.38E-07 | 3.45E-08 |
|    | 4.54E-17   | 4.98E-14 | 2.43E-05 | 3.37E-08 | 9.78E-17   | 2.69E-13 | 7.32E-07 | 5.27E-08 |
| 24 | 8.07E-17   | 1.43E-17 | 5.44E-06 | 1.41E-09 | 1.47E-16   | 2.33E-16 | 3.00E-07 | 9.52E-09 |
|    | 1.12E-16   | 4.05E-17 | 1.59E-05 | 1.19E-08 | 9.41E-17   | 5.79E-16 | 4.36E-07 | 1.41E-08 |
| 36 | 2.21E-16   | 4.94E-17 | 4.39E-06 | 9.04E-10 | 3.69E-16   | 1.22E-15 | 2.14E-07 | 4.57E-09 |
|    | 3.51E-16   | 3.82E-17 | 1.24E-05 | 6.42E-09 | 2.84E-16   | 2.28E-15 | 3.23E-07 | 6.62E-09 |
| 48 | 3.82E-16   | 1.34E-16 | 3.76E-06 | 6.40E-10 | 4.63E-16   | 8.80E-16 | 1.68E-07 | 2.74E-09 |
|    | 4.85E-16   | 1.30E-16 | 1.04E-05 | 4.15E-09 | 7.35E-16   | 1.46E-15 | 2.61E-07 | 3.90E-09 |

As one can see from Table 1, for smooth geometries like Figures 2(a) and 2(b), an accuracy of 16 digits can be achieved by directly applying the kernel splitting method with uniform discretization. However, for boundaries with corners, the singularity at the corner causes a significant loss of

accuracy. Such a loss cannot be improved by simply increasing the number of panels, as it greatly increases the number of unknowns and the condition number.

**5.2. Example 2: Elastic scattering with non-uniform meshes.** In this example, we test the elastic scattering problems for the droplet by non-uniform discretization. As compared to the last example, we refine the boundary near the corner by graded mesh and compute the numerical solutions by RCIP with different refinement numbers  $n_{sub}$ . The results for the exterior problems are shown in Figure 3.

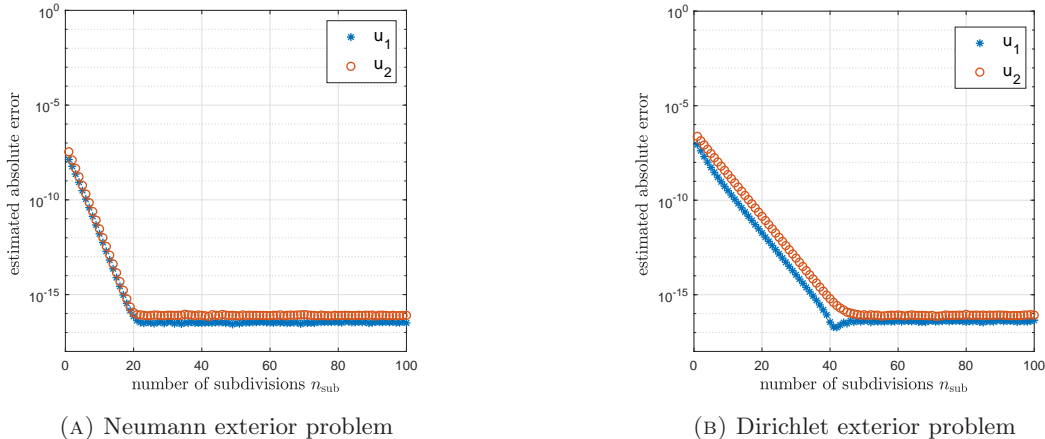


FIGURE 3. Exterior elastic scattering problems from a droplet. A graded mesh is applied to the neighborhood of the corner and RCIP is used to solve the resulted linear system.

As one can see from Figure 3, with an increasing mesh refinement near the corner, the accuracy has been steadily improved and finally stabilized at the machine accuracy. One interesting fact from Figure 3 is that the convergence rate of Neumann exterior problem is much faster than that of Dirichlet exterior problem. This is slightly counterintuitive since the solution for the Neumann problem with single layer potential is more singular than the solution for the Dirichlet problem with double layer potential [30]. However, for the interior problems, the solution for the double layer potential does converge faster than that of the single layer potential, as shown in Figure 4. In both cases, the accuracy reaches the machine precision and stays there when the number of subdivisions increases, which implies the proposed method is very stable for the resulted linear system.

**5.3. Example 3: Elastic scattering at different wavenumbers.** In this example, we test the exterior Dirichlet elastic scattering problems from a sector at different angular frequencies  $\omega$ , namely, from  $\omega = 3$  to  $\omega = 100$ , and choose to represent the solution by the combined layer potential (19) to avoid possible resonances. The corresponding numerical results are given in Table 2. It is well known that the higher the frequency, the more oscillatory the solution becomes, which requires finer mesh to resolve the solution. In this numerical experiment, one can find that once the oscillation is well resolved, the proposed scheme reaches the machine precision in all the frequencies that are tested.

We also consider incidence of the compressional plane wave with incident angle  $\theta = \pi/4$ . The density functions for different frequencies are shown in Figure 5. Based on the parametrization equation (61), the corresponding corner points are located at  $s = 0, 1, 2$  (and 3 is the same as 0 due to the periodicity) and one can clearly see that the solution  $\varphi_{coa}$  has jumps at these points and becomes highly oscillatory as the frequency increases.



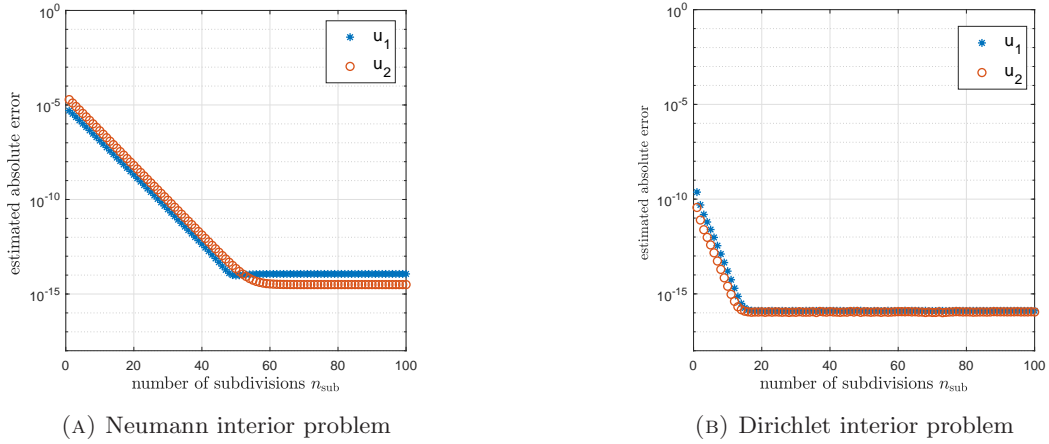


FIGURE 4. Interior problems for the elastic scattering in a droplet. A graded mesh is applied to the neighborhood of the corner and RCIP is used to solve the resulted linear system.

TABLE 2. Results for the elastic scattering of a sector at different wave frequencies

| N  | $n_{sub}$ | Absolute Error |               |               |               |                |
|----|-----------|----------------|---------------|---------------|---------------|----------------|
|    |           | $\omega = 3$   | $\omega = 10$ | $\omega = 30$ | $\omega = 50$ | $\omega = 100$ |
| 24 | 10        | 8.57E-14       | 1.08E-12      | 1.51E-12      | 1.42E-13      | 8.59E-09       |
|    |           | 3.60E-13       | 1.18E-12      | 6.15E-13      | 1.24E-11      | 1.02E-08       |
|    | 20        | 2.37E-16       | 9.98E-17      | 1.11E-16      | 7.77E-12      | 8.59E-09       |
|    |           | 2.28E-16       | 4.31E-17      | 7.63E-17      | 5.02E-12      | 1.02E-08       |
| 36 | 10        | 4.62E-14       | 5.77E-13      | 8.09E-13      | 4.13E-12      | 8.20E-12       |
|    |           | 1.92E-13       | 6.30E-13      | 3.29E-13      | 6.80E-12      | 1.93E-11       |
|    | 20        | 1.73E-16       | 1.67E-15      | 9.28E-17      | 2.89E-15      | 8.59E-12       |
|    |           | 6.13E-16       | 2.06E-16      | 6.34E-17      | 8.32E-15      | 1.84E-11       |
| 72 | 10        | 1.24E-14       | 1.97E-13      | 2.79E-13      | 1.42E-12      | 3.97E-13       |
|    |           | 6.30E-14       | 2.16E-13      | 1.13E-13      | 2.33E-12      | 1.97E-12       |
|    | 20        | 3.56E-15       | 2.45E-15      | 8.69E-17      | 4.27E-16      | 6.82E-16       |
|    |           | 3.29E-15       | 3.07E-16      | 5.02E-17      | 1.28E-16      | 8.59E-16       |

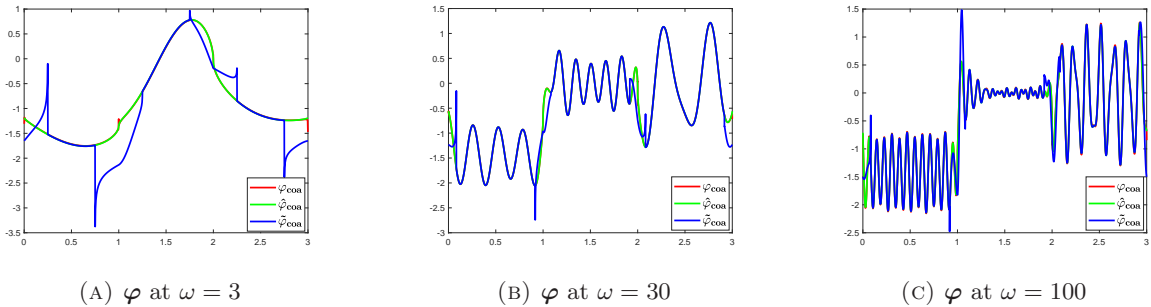


FIGURE 5. Density functions at different wave frequencies for the exterior elastic scattering problems from a sector. Here we only show the real part of  $\varphi_1$  in the elastic integral equations.

**5.4. Example 4: The leading asymptotic behavior of the density functions.** As we have observed from Figure (5), the density function of boundary integral equations exhibits a certain singularity that resembles the power solution (8) near the corner point. The phenomenon has been

thoroughly analyzed for Helmholtz equations [30]. However, similar analysis on the density behavior for the elastic equations is still open. To have a more comprehensive understanding on this singularity behavior, at least numerically, we evaluate the density function on the refined mesh in the vicinity of the corner. The recursively compressed inverse preconditioning allows us to recover the information on the fine grid through the backward recursion. This provides a scheme to calculate the value of the density function near the corner point and its asymptotic behavior. The detailed process of the reconstruction for  $\varphi$  can be found in [15, section 10]. Here we still consider the elastic scattering from a sector given by parametrization (61) with an opening angle  $\theta_0 = \frac{\pi}{2}$  and solve both the interior and exterior Neumann problems using single layer potential (21). Denote  $r$  the distance to the vertex of the sector on the boundary. Assume the leading asymptotic behavior of the density function  $\varphi$  to the boundary integral equation (22) is

$$\varphi(r) \sim O(r^\alpha), \quad r \rightarrow 0, \quad (62)$$

where  $\alpha > -1$  is the asymptotic order. Numerical results for the density functions of the interior and exterior problems near the corner point are shown in Figure 6. In particular, through curve fitting, we find the asymptotic order  $\alpha$  in these two cases are approximately equal to  $-0.3895$  and  $0.5408$ , respectively. We denote  $\alpha_{in} \approx -0.3895$  and  $\alpha_{ex} \approx 0.5408$  in (62) for the interior and exterior test problems.

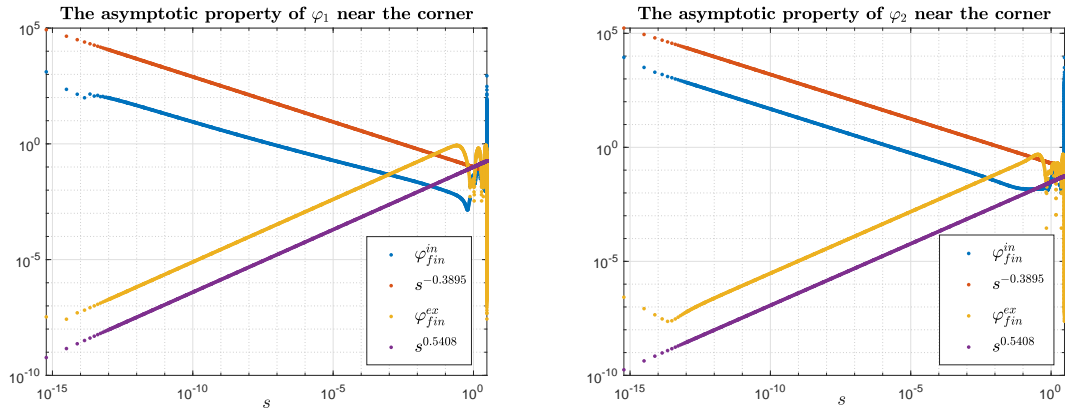


FIGURE 6. The asymptotic behavior of density functions in the neighborhood of the corner of a sector. The left and right are for  $\varphi_1$  and  $\varphi_2$  of the elastic integral equations, respectively.

On the other hand, the non-physical density  $\varphi$  for the second kind boundary integral equation (22) is related to the difference of some physical solutions of the interior and exterior Dirichlet problems of the sector  $\Omega$ . More specifically, assume we solve equation (22) for the interior Neumann problem and find the corresponding Dirichlet data  $\mathbf{u}_{in}^{sc}$  and Neumann data  $\mathcal{T}\mathbf{u}_{in}^{sc}$  on the boundary  $\partial\Omega$ . By Green's representation theorem [18], the scattered field  $\mathbf{u}_{in}^{sc}$  can be represented by

$$\mathbf{u}_{in}^{sc}(\mathbf{x}) = S[\mathcal{T}\mathbf{u}_{in}^{sc}] - D[\mathbf{u}_{in}^{sc}], \quad \text{with } \mathbf{x} \in \Omega. \quad (63)$$

Let us solve an exterior elastic scattering problem with Dirichlet data  $\mathbf{u}_{in}^{sc}$  on the boundary, and for that exterior problem, denote  $\mathbf{u}_{ex}^{sc}$  and  $\mathcal{T}\mathbf{u}_{ex}^{sc}$  the corresponding Dirichlet and Neumann data, respectively. By Green's representation theorem again, it holds

$$0 = S[\mathcal{T}\mathbf{u}_{ex}^{sc}] - D[\mathbf{u}_{ex}^{sc}], \quad \text{with } \mathbf{x} \in \Omega. \quad (64)$$

Subtracting (64) from (63) and using the fact that  $\mathbf{u}_{in}^{sc} = \mathbf{u}_{ex}^{sc}$  on  $\partial\Omega$ , we obtain

$$\mathbf{u}_{in}^{sc} = S[\mathcal{T}\mathbf{u}_{in}^{sc} - \mathcal{T}\mathbf{u}_{ex}^{sc}].$$

Compared to the single layer representation (21), one can conclude from uniqueness theorem that the density function  $\varphi$  is

$$\varphi = \mathcal{T}\mathbf{u}_{in}^{sc} - \mathcal{T}\mathbf{u}_{ex}^{sc}. \quad (65)$$

In other words, the density function  $\varphi$  for the single layer potential (21) is physically related to the Neumann data of the interior and exterior scattering problems that share the same Dirichlet data. Similar analysis applies to the exterior test problem. Therefore, to find the leading order coefficient  $\alpha$ , one only needs to analyze the behavior of the elastic field under Dirichlet boundary conditions.

It was shown in [27] that for a corner with opening angle  $\theta$ , the power in the solution (8) is related to the root  $\nu$  (with positive real part) of a transcendental equation. In the rigid boundary case, the equation is

$$\nu^2(1/(3 - 4\xi)^2)\sin^2(\theta) - \sin^2(\nu\theta) = 0, \text{ with } \xi = \frac{\lambda}{2(\lambda + \mu)}. \quad (66)$$

Due to the traction operator, the leading order singularity for the Neumann data in (65) is on the order of  $\nu - 1$ .

In our case, for the interior test problem, since  $\mathcal{T}\mathbf{u}_{in}^{sc}$  is smooth, the leading order singularity of  $\varphi$  is the same as the exterior Neumann data  $\mathcal{T}\mathbf{u}_{ex}^{sc}$ . We thus have to consider  $\theta = 3\pi/2$  in (66), where the first positive root is  $\nu_{in} = 0.61049131527757 \dots$ . According to the numerical results from Figure 6, it holds  $\alpha_{in} \approx -0.3895 \approx \nu_{in} - 1$  for the interior problem. Similarly, for the exterior test problem, the first positive root to (66) with  $\theta = \pi/2$  is  $\nu_{ex} = 1.540816086021658 \dots$  and it holds  $\alpha_{ex} \approx 0.5408 \approx \nu_{ex} - 1$ . Thus we have numerically verified the leading order coefficient for the density functions. This result will be useful for designing more effective numerical schemes based on the asymptotic expansion near the corner [30]. Nevertheless, it remains a qualitative result here without detailed analysis. It is one of our future work to explore more details between the asymptotic coefficients of boundary integral equations and the opening angle of the corner.

## 6. CONCLUSION

In this paper, we propose an effective solver for the elastic scattering with cornered domains. Our approach is founded upon an explicit decomposition of the kernel functions of the boundary integral operators. A high-order singular quadrature scheme is proposed by the composite Gauss-Legendre nodes and modified singular integrals. Subsequently, we employ the RCIP method to efficiently solve the resulting linear system arising from cornered domains. Numerical experiments demonstrate that the proposed method is efficient, stable and highly accurate in various geometries and boundary conditions. Furthermore, we verify the leading order singular asymptotic behavior of the density functions of boundary integral operators near the corner, which aligns with theoretical formulas. Future work includes the convergence analysis of the proposed scheme and its applications to the inverse elastic scattering problems.

**Acknowledgment:** The authors would like to thank Professor Shidong Jiang at Flatiron Institute for many helpful discussions.

## REFERENCES

- [1] Habib Ammari, Elie Bretin, Josselin Garnier, Hyeonbae Kang, Hyundae Lee, and Abdul Wahab. *Mathematical Methods in Elasticity Imaging*. Princeton University Press, 2015.
- [2] Kendall E Atkinson. *The numerical solution of integral equations of the second kind*, volume 4. Cambridge University Press, 1997.
- [3] Gang Bao, Liwei Xu, and Tao Yin. An accurate boundary element method for the exterior elastic scattering problem in two dimensions. *Journal of Computational Physics*, 348:343–363, 2017.
- [4] Eemeli Blåsten, Lassi Päiväranta, and John Sylvester. Corners always scatter. *Communications in Mathematical Physics*, 331:725–753, 2012.

- [5] Marius Bochniak and Fioralba Cakoni. Domain sensitivity analysis of the elastic far-field patterns in scattering from nonsmooth obstacles. *Journal of mathematical analysis and applications*, 272(1):318–334, 2002.
- [6] James Bremer. On the Nyström discretization of integral equations on planar curves with corners. *Applied and Computational Harmonic Analysis*, 32(1):45–64, 2012.
- [7] James Bremer, Zydrunas Gimbutas, and Vladimir Rokhlin. A nonlinear optimization procedure for generalized gaussian quadratures. *SIAM Journal on Scientific Computing*, 32(4):1761–1788, 2010.
- [8] Fanbin Bu, Junshan Lin, and Fernando Reitich. A fast and high-order method for the three-dimensional elastic wave scattering problem. *Journal of Computational Physics*, 258:856–870, 2014.
- [9] David Colton and Rainer Kress. *Integral equation methods in scattering theory*. Society for Industrial and Applied Mathematics, 2013.
- [10] Heping Dong, Jun Lai, and Peijun Li. Inverse obstacle scattering problem for elastic waves with phased or phaseless far-field data. *SIAM Journal on Imaging Sciences*, 2018.
- [11] Heping Dong, Jun Lai, and Peijun Li. A highly accurate boundary integral method for the elastic obstacle scattering problem. *Math. Comput.*, 90:2785–2814, 2020.
- [12] Charles L. Epstein and Michael O’Neil. Smoothed corners and scattered waves. *SIAM Journal on Scientific Computing*, 38(5):A2665–A2698, 2016.
- [13] Pierre Grisvard. *Elliptic Problems in Nonsmooth Domains*. Society for Industrial and Applied Mathematics, 2011.
- [14] Johan Helsing. Integral equation methods for elliptic problems with boundary conditions of mixed type. *Journal of Computational Physics*, 228(23):8892–8907, 2009.
- [15] Johan Helsing. Solving integral equations on piecewise smooth boundaries using the RCIP method: a tutorial. In *Abstract and Applied Analysis*, volume 2013. Hindawi, 2013.
- [16] Johan Helsing and Rikard Ojala. Corner singularities for elliptic problems: Integral equations, graded meshes, quadrature, and compressed inverse preconditioning. *Journal of Computational Physics*, 227(20):8820–8840, 2008.
- [17] George C Hsiao and Wolfgang L Wendland. *Boundary integral equations*. Springer, 2008.
- [18] R.J Knops. Three-dimensional problems of the mathematical theory of elasticity and thermoelasticity (vd kupradze, tg gegelia, mo basheleishvili, and tv burchuladze). *SIAM Review*, 23(4):543–545, 1981.
- [19] Rainer Kress. *Linear integral equations*, volume 82. Springer, 1989.
- [20] Rainer Kress. A Nyström method for boundary integral equations in domains with corners. *Numerische Mathematik*, 58:145–161, 1990.
- [21] V.D. Kupradze, T.G. Gegelia, M.O. Basheleishvili, and T.V. Burchuladze. *Three-dimensional problems of the mathematical theory of elasticity and thermoelasticity*, volume 25. North-Holland Publishing Company, 1979.
- [22] Jun Lai and Heping Dong. A fast solver for elastic scattering from axisymmetric objects by boundary integral equations. *Advances in Computational Mathematics*, 48(3):1–30, 2022.
- [23] Jun Lai and Peijun Li. A framework for simulation of multiple elastic scattering in two dimensions. *SIAM Journal on Scientific Computing*, 41(5):A3276–A3299, 2019.
- [24] Jun Lai and Jinrui Zhang. Fast inverse elastic scattering of multiple particles in three dimensions. *Inverse Problems*, 38(10):104002, sep 2022.
- [25] Frédérique Le Louër. A high order spectral algorithm for elastic obstacle scattering in three dimensions. *Journal of Computational Physics*, 279:1–17, 2014.
- [26] Peijun Li and Xiaokai Yuan. An adaptive finite element DtN method for the elastic wave scattering problem. *Numer. Math.*, 150:993–1033, 2022.
- [27] Yasir Nadeem Anjam and Akhtar Ali. On singularities of solution of the elasticity system in a bounded domain with angular corner points. *Mathematical Methods in the Applied Sciences*, 45(5):3124–3143, 2022.
- [28] Frank WJ Olver, Daniel W Lozier, Ronald F Boisvert, and Charles W Clark. *NIST handbook of mathematical functions hardback and CD-ROM*. Cambridge university press, 2010.
- [29] Anna-Margarete Sändig, Uwe Richter, and Rainer Sändig. The regularity of boundary value problems for the lamé equations in a polygonal domain. *Rostocker Mathematisches Kolloquium*, 36, 01 1989.
- [30] Kirill Serkh and Vladimir Rokhlin. On the solution of the helmholtz equation on regions with corners. *Proceedings of the National Academy of Sciences*, 113:9171 – 9176, 2016.

SCHOOL OF MATHEMATICAL SCIENCES, ZHEJIANG UNIVERSITY, HANGZHOU, ZHEJIANG 310027, CHINA  
 Email address: yaojianan@zju.edu.cn

SCHOOL OF MATHEMATICAL SCIENCES, ZHEJIANG UNIVERSITY, HANGZHOU, ZHEJIANG 310027, CHINA  
 Email address: baolingxie@zju.edu.cn

SCHOOL OF MATHEMATICAL SCIENCES, ZHEJIANG UNIVERSITY, HANGZHOU, ZHEJIANG 310027, CHINA  
 Email address: laijun6@zju.edu.cn

